Title

MPC solution for optimal load shifting for buildings with ON/OFF staged packaged units: Experimental demonstration, and lessons learned

Authors

Kim, Donghun

Braun, James E

Publication Date

2022-07-01

DOI

10.1016/j.enbuild.2022.112118

Peer reviewed

MPC Solution for Optimal Load Shifting for Buildings with ON/OFF Staged Packaged Units: Experimental Demonstration, and Lessons Learned

Donghun Kim[a,*], James E. Braun[b]

[a]*Building Technology & Urban Systems Division, Lawrence Berkeley National Laboratory, Berkeley, CA, USA*
[b]*School of Mechanical Engineering, Purdue University, West Lafayette, IN, USA*

Abstract

Small and medium-sized commercial buildings (SMCB) are significant demand response resources, and it is important to develop grid-responsive control algorithms that exploit those resources and create financial benefits for building owners and HVAC service providers. Furthermore, unlike large-sized commercial buildings, there is an opportunity to have universally applicable control solutions for many SMCBs since those buildings have a consistent HVAC system configuration: SMCBs are commonly served by multiple-staged air conditioning units controlled by their own thermostats. Despite the demand response potential and scalability, however, very few control solutions are available for SMCBs. Typical model predictive control (MPC) and heuristic control approaches for cooling load shifting that lower thermostat setpoints before an electric price jump are suitable mainly for large-sized commercial buildings where a continuous capacity modulation is possible, e.g., via dampers in variable air volume terminal units. However, those approaches can cause undesired, high peaks for SMCBs due to the nature of ON/OFF unit staging and narrow thermostat deadbands. This could discourage the use of advanced grid-responsive controls for SMCBs due to the concern of high demand charges, and has to be resolved. This paper presents a MPC solution that overcomes this challenge. It has a hierarchical MPC structure where an upper level MPC is responsible for electrical load shifting in response to an electric price signal while a lower level MPC is responsible for coordinating compressor stages to eliminate unnecessary peaks and follows the setpoints determined by the upper level MPC. Two one-month, comprehensive laboratory tests have been carried out to demonstrate load shifting and cost savings for the algorithm. Interesting trade-offs between energy efficiency and load flexibility were observed and are discussed, and lessons learned for applying MPCs for SMCBs are also presented.

Keywords: Model predictive control, staged units, packaged air conditioner, load shifting, load flexibility

NOMENCLATURE

CT: current transducer

EER: energy efficiency ratio

HVAC: heating, ventilating, and air conditioning

IO: inputs and outputs

*Corresponding author
Email address: donghunkim@lbl.gov (Donghun Kim)

NOAA: national oceanic and atmospheric administration

RMS: root mean squares

RTU: rooftop unit

SMCB: small and medium-sized commercial buildings

TOU: time of use

$(A(\cdot), B_u(\cdot), B_{T_o}(\cdot), C(\cdot))$ **:** a state space model structure that maps θ to building dynamics, i.e. G_u and G_{T_o}

e **:** one step ahead prediction error

$(\mathcal{F}(\cdot), \mathcal{G}(\cdot))$ **:** a state space model structure that maps ρ to lumped disturbance dynamics , i.e. H

G_u **:** dynamic system that maps u to y

G_{T_o} **:** dynamic system that maps T_o to y

H **:** dynamics of lumped output disturbances

k **:** current time step

j **:** prediction time step

m **:** number of measured inputs

p_i**:** i^{th} unit power

N_p **:** prediction horizon

n **:** number of RTUs

$\dot{Q}_g$ **:** unmeasured heat gains

(T_l, T_u)**:** lower and upper temperature bounds

T_o **:** outdoor air temperature

u_i**:** i^{th} unit stage

u **:** vector of RTU compressor stages

v **:** lumped output disturbances

$\hat{x}_a$**:** aggregated state that includes building temperatures and internal state of disturbances

y **:** vector of thermostat temperatures

(Γ_l, Γ_u) **:** temperature violations from lower and upper temperature bounds

δ **:** an upper bound of instantaneous power

ζ**:** internal state of lumped output disturbances

θ **:** physical parameters consisting of thermal resistances and capacitances

ρ **:** parameters that constructs dynamics of lumped output disturbances, i.e. H

(ω_l, ω_u)**:** weights on optimization variables for (Γ_l, Γ_u)

ω_d **:** weight on optimization variables for δ

1. Introduction

Since buildings account for over 70% of U.S. total electricity use (U.S. Energy information administration), and contribute significantly to electric power demand peaks and carbon emission, integrating building controls with the grid can improve grid reliability, resiliency, and efficiency, and help in achieving states' and government's carbon neutrality goals. Buildings have inherent energy storage, i.e., the thermal mass associated with building structure, which can be used for shifting and shedding significant thermal loads. The use of thermal mass in cooling seasons can involve pre-cooling the building prior to an event (e.g., an ON peak price period) in order to lower cooling load and electric peak demand during the event. One of the most popular and widely studied control approaches for managing thermal mass is model predictive control (MPC), and a large number of previous studies have demonstrated that it can provide grid services while presenting economic benefits to building owners without compromising thermal comfort.

MPC is a control technique that involves the utilization of mathematical models and forecasts to optimize the operation of a given system. Historically developed from the chemical process industry, applications of MPC to buildings have gained significant attentions for the last several decades since the early 1990's (Braun, 1990) for multiple purposes. Candanedo et al. (2013) carried out a simulation study of applying MPC, for a case study building which has two 3 stage chillers and an ice storage tank, to minimize the energy cost (with no demand charge). The MPC achieved from 5 to 20% energy cost savings. Oldewurtel et al. (2011) developed a linear-MPC for office buildings in Zurich, and reduced the peak demand by 3.5% without battery and 17.5% with battery in simulation studies. Risbeck et al. (2017) extends MPC for a more complex energy system to minimize utility costs. Ceusters et al. (2021) developed a mixed-integer linear-MPC to optimize the operation of an energy system with renewable generation (PV), and battery. Other example applications of MPC to building energy systems, we refer to (Avci et al., 2013; Bianchini et al., 2017) for demand-response problems with real-time pricing, (Oldewurtel et al., 2010) for reducing electrical peak demand, (Patteeuw et al., 2016; Qureshi and Jones, 2018) for increasing flexibility and sustainability of energy systems with renewable generation, and (Bianchini et al., 2016; Vrettos et al., 2013) for a pricing-formulation. Recently, a MPC application and demonstration for reducing carbon emission while minimizing peak demand for a central cooling plant is also reported (Kim et al., 2022). Hilliard et al. (2016); Rockett and Hathway (2017) summarized applications, challenges and future research topics of MPC for commercial buildings. Similarly, Killian and Kozek (2016) provided future trends and potentials for general building markets. In addition, it summarized technical questions and MPC challenges including high efforts for modeling, lack of tools for automating the modeling process, and shortage of modeling & control experts in the HVAC domain. We refer to (Drgoňa et al., 2020) for a more recent and comprehensive review on MPC for buildings which covers a variety of technical aspects of MPC including modeling approaches (e.g., system identification and machine learning methods), state estimators (e.g., Kalman filter and Moving horizon estimator), mathematical MPC problem classes (e.g., Linear MPC and nonlinear MPC), MPC architectures for HVAC systems (e.g., centralized MPC and distributed MPC), and software tools for building modeling, simulation and control.

Small-sized ($< 464\ m^2$, $< 5,000\ ft^2$) and medium-sized ($< 4,640\ m^2$, $< 50,000\ ft^2$) commercial buildings (SMCB) account for about 95% of U.S. commercial buildings, 50% (3.6 billion m^2) of the total commercial indoor floor space and 60% of energy usage in the commercial building sector. Thus, SMCBs are undoubtedly tremendous, readily-available demand response resources. Furthermore, unlike large-sized commercial buildings, SMCBs have a fairly consistent HVAC and control configuration: commonly served by multiple staged air conditioning units, e.g., rooftop units (RTU), for space heating and cooling where each unit stage is controlled by its own thermostat. Examples are banks, retail stores, restaurants, schools and factories. This implies that there is a potential to have a universal and scalable control solution which can be applied to many SMCBs and could rapidly transition them to Grid-interactive Efficient Buildings (GEB).

Surprisingly, however, SMCBs have not been a major focus for building control researchers in the past[1] despite a large number of MPC studies and the large potential as flexible load resources. Most studies for SMCBs have focused on improving the energy efficiency of individual RTUs by the use of variable speed fans and compressors (Cai and Braun, 2018; Wang et al., 2019), economizer controls, and integrated controls. Taylor and Cheng (2010) investigated when to switch the economizer mode depending on U.S. climate zones. Seem and House (2010) developed an optimization-based economizer control and compared it with typical economizer controls, e.g. differential dry-bulb temperature controls, for various climates. Wang et al. (2013) developed an integrated control, namely Advanced Rooftop Control (ARC), which consists of integrated air-side economizer controls, supply-fan speed controls, cooling capacity controls and demand-controlled ventilation controls, and provided site evaluation results.

Only a limited number of MPC papers are found in the literature for SMCBs. Nutaro et al. (2014) developed a MPC algorithm and implemented it at a gymnasium having four identical 10-ton RTUs. This coordinator combines a simplified ARX type input-output model with heuristics and optimization to limit electric peak demand. The reduction of peak power consumption was about 15% with respect to a conventional thermostat control for the building. Kim et al. (2015) developed a MPC algorithm for minimizing energy consumption and electric peak demand for multiple RTUs especially for open-spaced buildings. The control approach was designed to minimize sensor and configuration requirements in order to enable a more cost effective control implementation for small/medium commercial buildings. It was implemented at a laboratory and multiple field sites, and reported overall up to 10% building HVAC energy savings and 20% peak demand reduction (Kim and Braun, 2018). Biyik et al. (2015) developed a RTU coordinator to minimize peak power. The goal was achieved by assigning different time varying penalties to different RTUs in order to prevent all units from operating simultaneously. It is reported that the peak power reduction with the optimal control strategy was about 20-40% for existing buildings. Putta et al. (2015) applied dynamic programming to solve an optimization problem for minimizing energy consumption and reducing compressor short cycling. In the case study, about 10% energy savings were estimated for a building served by 4 RTUs. Zhang et al. (2017) developed a RTU coordination control algorithm that shaves power usage within a limit during a demand response event for 90 minutes when triggered by a utility company, while minimizing comfort impacts.

However, those studies focus mainly on peak demand reduction and energy efficiency not load flexibility. SMCBs have a unique technical difficulty in load shifting. Typical MPC approaches in the literature, for variable air volume systems for example, which lower thermostat setpoints to shift load would not work for

[1]This might be because SMCBs do not typically have building automation systems (according to Katipamula et al. (2012), over 90% of small and medium-sized commercial buildings do not have a building automation system) and because the cost savings opportunities relative to implementation costs have been small. However, the situation is changing because of the availability of low-cost, web-enabled smart thermostats and other devices (e.g., smart plugs) that have emerged in the marketplace in the past few years.

the type of buildings. This is because when the setpoints are lowered by, e.g., a couple of degree Celsius, full compressor stages for all units would be simultaneously activated creating a high electric peak due to the nature of ON/OFF stage of the units and narrow thermostat deadbands (usually $< 1^oC$). This is a very significant issue, since the undesired high peak and hence potentially high demand charge to building owners makes no economic sense for load shifting. To fully exploit SMCBs' demand response resources, this problem has to be solved.

This paper develops and demonstrates a MPC solution for SMCBs to overcome this problem. The solution incorporates a hierarchical MPC approach. Long-term experiments were carried out to demonstrate the load shifting and demand reduction capabilities. The MPC behaviors under two different time of use (TOU) scenarios were investigated. Interesting trade-offs between energy efficiency and load flexibility were observed and are discussed.

2. System Description and MPC Challenge

A packaged air conditioning unit consists of a vapor compression system, supply air blower and duct, air mixing box and optional economizer and heating element, i.e. an electric heater or gas furnace. In general, a thermostat is dedicated to a unit and turns one or more compressor stages on and off to maintain the thermostat temperature near a setpoint. The first stage is typically energized when the thermostat temperature rises above the setpoint by a deadband. If the temperature continues to rise and exceeds the setpoint by a 2nd stage deadband, then the 2nd stage compressor is energized. The supply fan is typically on continuously during the occupied period and will cycle with the compressor during unoccupied times. Most packaged units for small and medium-sized commercial buildings do not have variable-speed compressors due to economic considerations.

In developing the MPC, we define the following nomenclature.

n**:** number of thermostats or equivalently the number of staged units

y_i**:** thermostat temperatures for the i^{th} unit

y**:** a vector of thermostat temperatures ($\in \mathbb{R}^n$)

u_i**:** compressor stage (control input) for i^{th} unit. For a single-stage unit, it is either 0 or 1, For a two-stage unit, it could be 0,1 or 2.

u**:** a vector of unit stages, i.e., $u = [u_1, u_2, \cdots, u_n]^T$

T_{oa}**:** outdoor air temperature

Let $[u^T, T_o]^T$ be the inputs having the size of m where $m = n + 1$. The dynamic system that maps the compressor stages and outdoor air temperatures to thermostat temperatures is denoted as $y = G_u \circ u + G_{T_o} \circ T_o + v$ where $G_u : u \mapsto y$ and $G_{T_o} : T_o \mapsto y$ respectively, and v represents the unmeasured disturbances and model mismatch.

The MPC challenge associated with load shifting for buildings served by multiple staged units is discussed using the field results presented in Fig. 1. The building is a typical small retail store (floor area around 1,400 m^2, 15,000 ft^2) and has 4 RTUs (rooftop units) where three of them, named U1-3, serve a main open service area and one RTU, named U4, serves a storage room. U1, U2 and U3 are two-stage units while U4 is a single-stage unit. The profiles of thermostat temperatures, compressor stages and total HVAC power consumption are shown in the figure. For each unit, the compressor run time over a 5-minute interval is used to estimate compressor stages (the 2nd subfigure). At the arrowed point, the setpoints changed from

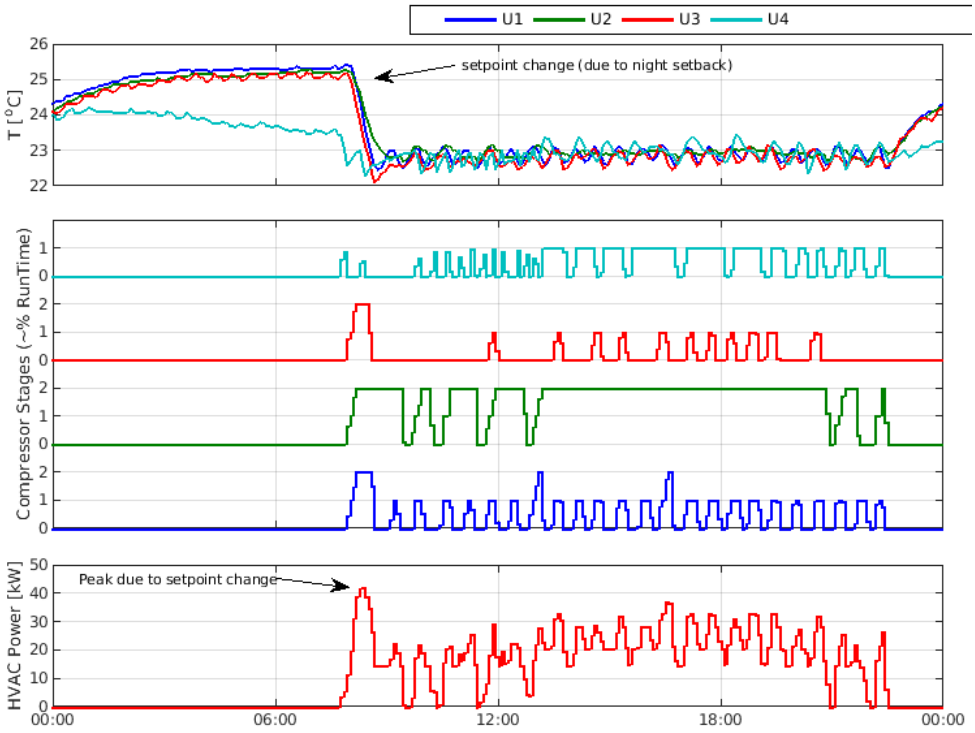

Figure 1: Field data showing the MPC challenge of an unnecessary peak caused by abrupt setpoint changes

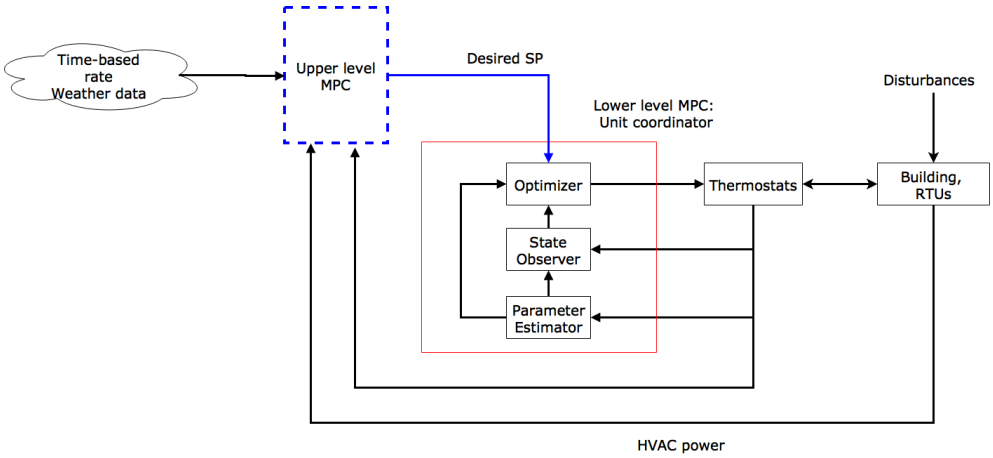

Figure 2: Conceptual diagram of a two-layer MPC for optimal load shifting and further peak demand reduction

about 25.5^oC (78^oF) to 22.2^oC (72^oF) according to thermostat night setback schedules. Note that U1 to U3 ran with full stages (the 2nd subfigure) and the total HVAC power peaked (the 3rd subfigure) at the time. Even greater peaks could occur for load-shifting strategies than for the return from night setup because of higher non-HVAC power during a pre-cooling period. Although the challenge of reducing these peaks seems straightforward, it is surprising that very few papers discussed and attempted to resolve it in the MPC literature.

3. Methodology: Hierarchical MPC Design

The proposed MPC for optimal load shifting for SMCBs has a hierarchical control structure as shown in Fig. 2 in which the upper level MPC (UMPC) marked with the blue dashed box optimizes desired setpoints while the lower level MPC (LMPC) marked with the red box acts as a slave controller. The UMPC is responsible for the optimal load shifting in response to utility price and weather signals by looking at long-term building thermal dynamics, while the LMPC optimally coordinates multiple RTUs or other unit packages to track the optimal setpoints determined by the UMPC while preventing unnecessary peaks discussed in the previous section.

3.1. Design of Lower MPC

In this section, mathematical descriptions of the LMPC are presented. It should be noted that the prediction horizon of the LMPC (N_p^L) is relatively short, e.g. 30 min to 1 hour. The control problem at a current time step k is:

$$\begin{aligned} \min \quad & \sum_{j=1}^{N_p^L} \sum_{i=1}^{p} P_i u_i(k+j-1) + \omega_d \delta + \omega_l \Gamma_l + \omega_u \Gamma_u \\ s.t. \quad & T_l^L - \Gamma_l \leq E(y(k+j)|\mathcal{G}_k) \leq T_u^L + \Gamma_u \\ & \sum_{i=1}^{p} P_i u_i(k+j-1) \leq \delta \quad (\forall j \in \{1, \cdots, N_p^L\}), \end{aligned} \tag{1}$$

where j represents the time step for control changes measured from the current value of k. $u_i(k+j)$ and $y_i(k+j)$ represent unit stage and thermostat temperature for the i^{th} unit at the $k+j^{th}$ timestep. P_i is the rated power for the i^{th} unit. $E(y(k+j)|\mathcal{G}_k)$ is the optimal j-step prediction of thermostat temperatures given data $\mathcal{G}_k = \{y(k-1), y(k-2), \cdots, u(k+j-1), u(k+j-2), \cdots\}$. The prediction is calculated using the identified model, G_u (See Section 4). $T_u^U (\in \mathbb{R}^n)$ are the desired setpoints that will be specified by the upper level MPC, and $T_u^L (\in \mathbb{R}^n)$ are temperature lower bounds. $\omega_l, \omega_u (\in \mathbb{R}^+)$ and $\omega_d (\in \mathbb{R}^+)$ are weights on variables of $\Gamma_l, \Gamma_u (\in \mathbb{R}^+)$ and $\delta (\in \mathbb{R}^+)$. Γ_l and Γ_u can be seen as comfort violations from the first constraint of (1) that are introduced to ensure a feasible solution. The variables to be optimized are the unit stages for all units over the prediction horizon and $\delta, \Gamma_l, \Gamma_u$, which form a mixed integer linear programming problem.

From the last constraint, it can be seen that δ is an upper bound on the electric demand for each time interval over the prediction horizon. Therefore, minimizing δ will naturally lower the electric peak demand over the prediction horizon. The coordination of unit stages to minimize the electric demand is the key component of the LMPC to eliminate high peaks for load shifting. For the capability of peak regulation and reliability of the LMPC, we refer to Kim and Braun (2018) which reports long-term field site MPC results.

3.2. Description of Upper MPC (UMPC)

In this section, mathematical descriptions of the UMPC are presented. To provide the optimal upper bounds (or desired cooling temperature setpoints) to the LMPC, i.e., T_u^L, it is natural to optimize setpoints by predicting a cost associated with the setpoints. However, it is challenging to obtain a dynamic model which maps setpoints to cooling load or power, because of the nonlinearity (hysteresis) of thermostats. Instead, an alternative approach is used: input trajectories are optimized first and desired setpoint trajectories are back calculated from the optimal inputs and G_u. With this in mind, the control problem of the UMPC at a current time step k is:

$$\min \quad \sum_{j=1}^{N_p^U} \sum_{i=1}^{p} R(k+j-1) P_i(k+j-1) \bar{u}_i(k+j-1) \tag{2}$$
$$+\omega_d \delta + \omega_l \Gamma_l + \omega_u \Gamma_u$$
$$s.t. \quad T_l^U - \Gamma_l \leq E(\bar{y}(k+j)|\mathcal{G}_k) \leq T_u^U + \Gamma_u \tag{3}$$
$$\sum_{i=1}^{p} P_i(k+j-1) \bar{u}_i(k+j-1) \leq \delta$$
$$0 \leq \bar{u}_i(k+j-1) \leq 1 \quad (\forall j \in \{1, \cdots, N_p^U\}),$$

where $\bar{u}$ and $\bar{y}$ are the moving averaged unit stages and thermostat temperatures, respectively, over a window (a 30-minute interval is used for this study). Because of averaging, $\bar{u}_i$ for each sampling time is a real number bounded by 0 and 1 (for a single stage unit): $\bar{u}$ can be viewed as unit runtime fractions (RTF) over the averaging window. A sequence of $\bar{u}(\cdot)$ is the optimization variable of (2). The desired setpoint trajectories are calculated with the optimal RTFs and an input-output model.

Differences compared with the LMPC formulation in (1) are explained as follows. N_p^U is the prediction horizon for the UMPC ($>$ 6 hours), which is longer than N_p^L of the LMPC (around 1 hour). The control implementation time for the UMPC is also longer than that of the LMPC: That is, the UMPC and LMPC are implemented for every 30 min and 5 min, respectively. R which is the electricity rate is provided only to the UMPC for load shifting. The feedback and future prediction data set, i.e. $\mathcal{G}_k$, includes forecast of

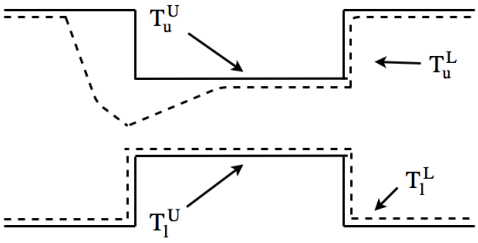

Figure 3: Example of upper and lower bounds for the UMPC and LMPC

outdoor air temperature as follows. $\mathcal{G}_k = \{\bar{y}(k-1), \bar{y}(k-2), \cdots, \bar{u}(k+N_p^U-1), \bar{u}(k+N_p^U-2), \cdots, \bar{T}_o(k+N_p^U-1), \bar{T}_o(k+N_p^U-2), \cdots\}$ where $\bar{T}_o$ is the moving averaged signal with the same window size for $\bar{u}, \bar{y}$.

The upper and lower temperature bounds, i.e. T_l^U, T_u^U indicate an acceptable temperature range specified by users and are different from the bounds for the LMPC. The bounds for the LMPC could be narrower than that of the UMPC and are determined by the UMPC as follows.

$$T_{u,i}^L(k) = \begin{cases} \bar{y}_i^*(k), & if\ \bar{u}_i^*(k) > 0 \\ T_{u,i}^U(k), & if\ \bar{u}_i^*(k) = 0 \end{cases} \tag{4}$$
$$T_{l,i}^L(k) = T_{l,i}^U(k),\ \forall i \in \{1, 2, \cdots, p\}$$

where $\bar{u}_i^*(k)$ indicates the optimal RTF over the averaging window for the i^{th} unit at the k^{th} timestep of the UMPC and $\bar{y}_i^*(k)$ is the corresponding desired temperature. The first equation of (4) means the desired temperature profiles are used for the upper bound for the LMPC. However, it is modified with the following heuristic strategy: if the UMPC does not use the i^{th} unit, i.e. $\bar{u}_i^*(k) = 0$, put the upper bound of the LMPC for the i^{th} unit as high as possible in order to turn off the unit.

Example profiles of the upper and lower bounds for the UMPC and LMPC are shown in Fig. 3. The bounds for the UMPC, solid lines in the figure, are based on a predefined temperature band while the bounds of the LMPC, dashed lines, follow a decision of the UMPC according to (4).

3.3. Basis of the Hierarchical Control Architecture

The control method is related to two successful and popular process control strategies, i.e. multilayer and cascade controls. A standard multilayer control (Skogestad and Postlethwaite, 2007, p.386) in process control assigns a different task to each layer. In general, lower (or control) layers, focus on setpoint tracking while upper (or optimization) layer(s), compute optimal setpoints in an economic sense. The optimization layer typically works with an open-loop static nonlinear model. The underlying idea of the control architecture is a time scale separation between the two layers, say a factor of five or more in terms of closed-loop responses. Our strategy is essentially the same as the standard hierarchical control except that both layers in our strategy seek economic benefits in different time scales and the UMPC works with a dynamic model with feedback information. In a technical sense, there is a similarity between the presented controller and a cascade controller, since both involve linear dynamic models that operate on different time scales. One of the most significant advantages of cascade control is that it can substantially improve control performance under disturbances and nonlinearities associated with the inner loop. This fact gives some confidence on the disturbance rejection performance of our control approach.

4. Methodology: Modeling

To predict zone air temperature profiles with a forecast for the outdoor air temperature and a candidate profiles of control inputs, we utilized a methodology termed the Lumped Disturbance modeling approach (LD) (Kim et al., 2016). We refer to Kim et al. (2018) for the mathematical description and background of the algorithm, and validation for the case study building of this paper. Instead, the key concept of the modeling approach is outlined in this section.

It starts with a typical thermal network model structure consisting of thermal resistances (Rs) and capacitances (Cs). However, for real buildings, the information of various heat gains, such as lighting, plug, occupancy loads and in/exfiltration, is often not available, and adding additional sensors to measure them for control purposes is cost prohibitive, especially for SMCBs. The imperfect building data set because of the missing information often leads to failure of conventional system identification approaches (e.g., (Braun and Chaturvedi; Li et al.)) that estimates physical parameters of a thermal network model by minimizing a norm of simulation errors. This is because the conventional identification scheme has to explain the input and output relationships (in our case, $G_u : u \mapsto y$ and $G_{T_o} : T_o \mapsto y$) without the missing heat gain information, and the only way of doing this is to bias the physical parameters. On the other hand, the LD approach aims at extracting an improved RC network building model from data under the presence of unknown heat gains. It models not only the thermal network but also dynamics of unmeasured disturbances.

A discretized thermal network system for our applications can be expressed as the following general form

$$y(k) = G_u(z)u(k) + G_{T_o}(z)T_o(k) + G_g(z)\dot{Q}_g(k) \tag{5}$$

where z^{-1} is the backward time shift operator such that $z^{-1}x(k) = x(k-1)$ for a sequence of x. $\dot{Q}_g(k)$ represents unmeasured heat gains [kW] that could include occupancy heat gain, lighting load and solar irradiation, and G_g is the corresponding transfer function that maps $\dot{Q}_g$ to y.

Once a RC-network model structure (e.g., 2R2C) is specified, a discrete time state space model for (5) can also be expressed as

$$\begin{aligned} T(k+1) &= A(\theta)T(k) + B_u(\theta)u(k) + B_{T,o}(\theta)T_o(k) + B_g(\theta)\dot{Q}_g \\ y(k) &= C(\theta)T(k). \end{aligned} \tag{6}$$

θ is the physical parameters for the RC network that need to be identified. T contains estimated states (temperatures of zones and walls in the RC network). $A(\theta), B_u(\theta), B_{T_o}(\theta)$ and $B_g(\theta)$ are defined by the RC network model and a discretization scheme, e.g. the zero-order hold. From (6), since $\dot{Q}_g$ is unknown, one can see the difficulty of estimating θ from u, T_o, y.

In the lumped disturbance modeling approach, a new signal v is defined as $v(k) := G_g(z)\dot{Q}_g(k)$, and named lumped output[2] disturbance, and try to model it as a stochastic process. A key observation is that v is a low pass filtered signal through the slow building dynamics of G_g, although input disturbances could have a variety of frequency contents. This suggests that v could be modeled as

$$v(k) = H(z)e(k) \tag{7}$$

with a low pass filter H. $e(\cdot)$ is a white noise process in the equation.

Therefore, the building system we wish to identify in the LD scheme has the following form rather than (5).

$$y(k) = G_u(z)u(k) + G_{T_o}(z)T_o(k) + H(z)e(k) \tag{8}$$

[2]Note from (5) that output disturbance v has the unit of $[^oC]$ while the input disturbances $\dot{Q}_g$ have that of $[kW]$ or $[kW/m^2]$.

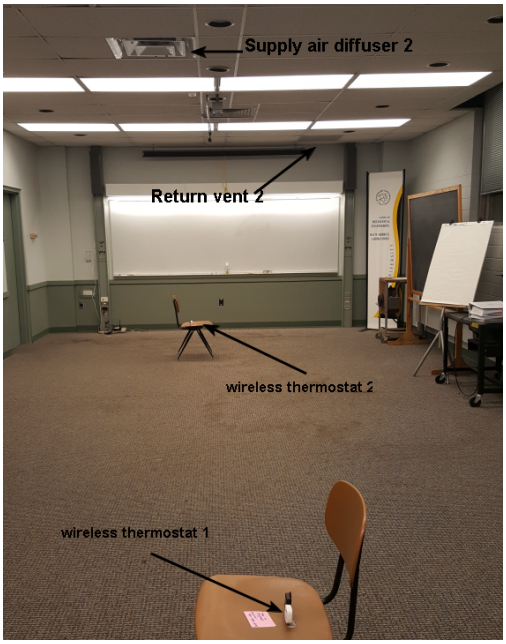

Figure 4: Case study building (supply air diffuser 1 and return vent 1 are not shown)

A discrete time state space model for (8) is

$$\begin{aligned} T(k+1) &= A(\theta)T(k) + B_u(\theta)u(k) + B_{T,o}(\theta)T_o(k) \\ y(k) &= C(\theta)T(k) + v(k) \\ \zeta(k+1) &= \mathcal{F}(\rho)\zeta(k) + \mathcal{G}(\rho)\epsilon(k) \\ v(k) &= \zeta(k) + \epsilon(k). \end{aligned} \tag{9}$$

ρ represents parameters for parameters for the low pass filter to characterize v. Like before, θ is physical parameters for a RC network model that consists of thermal resistances and capacitances. ζ and matrices of $(\mathcal{F}, \mathcal{G})$ represent the internal state and dynamics, respectively, appearing in converting the low pass filter H to the state space description (9). To retrieve θ and ρ from measurements of u, T_o, y, the prediction error method is used based on the state space form that minimizes a norm of the innovation process of ϵ in (9). The uniqueness of the LD modeling approach compared with other grey-box modeling approaches (Andersen et al., 2000; Braun et al., 2001; Chen et al., 2015; Dong et al., 2011; Fraisse et al., 2002; Harb et al., 2016; Reynders et al., 2014; Rogers et al., 2014; Širokỳ et al., 2011) is that building disturbances are not treated as white noise, but are modeled explicitly with ρ. We refer to Kim et al. (2018) for more detailed discussion and experimental validation for the case study building of this paper.

(a) (b)

Figure 5: (a) Floor plan with locations of thermostats, supply diffusers and return vents and (b) external view of the demonstration site (Purdue Herrick Laboratory)

5. Laboratory Test Results

5.1. Laboratory Environment Description

5.1.1. Site Description

A cooling system for a conference room (about 15 m long, 7 m wide and 3.5 m high) in the Ray W. Herrick Laboratories at Purdue University, IN, U.S. (see Fig. 4) was retrofitted to test the overall MPC approach. Two packaged air conditioners (termed U1 and U2) were installed and the air duct system was reconfigured accordingly. U1 is a 1-ton single stage unit with an energy efficiency ratio (EER) 9 and U2 is a 2-ton single stage unit with 10 EER. Thermostats, supply and return vents associated with the two units are shown in Fig. 4 and Fig. 5. Note that there is a strong coupling between the two sub-zones (or thermostats), and hence the operation of one unit can influence both thermostat temperatures. Unmeasured heat sources are lighting gains, loads from electric appliances (a small freezer and one laptop computer), infiltration/exfiltration, solar gains through windows, and occupancy gains. The lights were turned ON and OFF by occupant random behavior.

It should be noted that the conference room is not very representative of many SMCBs in the sense that 1) it has a carpet and mat (see Fig. 4) and 2) it has a high U-value for the wall and window (See the external view of Fig. 5): the external wall consists of pure bricks (without insulation) and single pane windows covering around 1/3 of the wall area. These system properties restrict the MPC savings potential which will be discussed in detail.

Current transducers (CT, model: CU-855) were installed to measure currents for the two packaged units. They convert true RMS 10 amps to 0-5 VDC for a single-phase AC power. The accuracy is $\pm$ 1% of 10 amps. The data was recorded through an Arduino board at 1 minute intervals. Unit powers were estimated using the CT with an assumption that the power factors and RMS voltage are reasonably constant.

The control platform for implementing MPC is shown in Fig. 6. The controller (i.e., the black box in the figure) communicates with individual thermostats and the MPC server. This work used low-cost ZigBee thermostats, and the thermostat signals, i.e. temperatures and unit stages, were recorded in the MPC server for a 5-min sampling time interval via the controller. The thermostat allows specifying either a temperature setpoint or compressor stage. When a setpoint is specified, an internal thermostat control with a usual

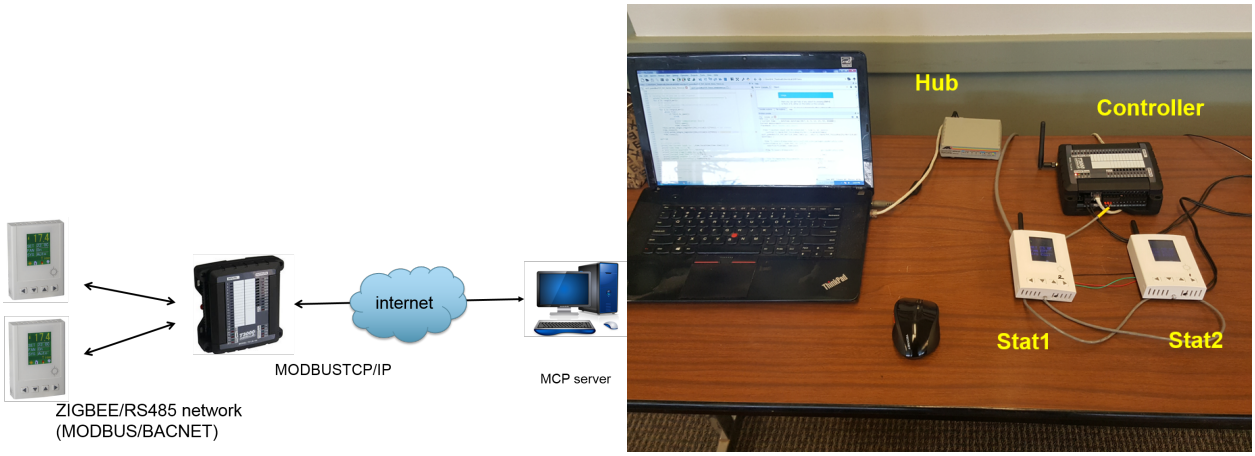

(a) (b)

Figure 6: (a) proposed MPC control/communication schematic and (b) experimental setup

1^oF (0.55^oC) deadband for the single-stage unit, and two 1^oF (0.55^oC) deadbands for the two-stage unit is applied.

5.1.2. Controller Setup, Implementation, and Performance Indexes

The state-of-the-art MPCs for SMCBs described in Introduction are not representative of what happens in the real world. There appear to be no commercial implementations of those controls, and commercial thermostat controls for packaged units are still based on a predefined setpoint schedule. In addition, they can not shift the cooling load as described in Introduction: that is, their response remains the same regardless of a utility price signal. Therefore, to demonstrate the load shifting capability (i.e., an optimized precooling in response to a utility price signal) while eliminating the unnecessary peak, we compared the proposed MPC to the following conventional control.

Conventional Control Set Up: A conventional thermostat control (Conv) turns on and off the unit stages based on thermostat deadband(s) and tracking error between the measured thermostat temperature and setpoint. The Conv follows a night setup schedule, 23.3^oC (74^oF) during the occupied period (9:00 AM to 6:00 PM) and 24.4^oC (76^oF) during the unoccupied period.

Hierarchical MPC Set Up: For the lower level MPC (LMPC), the sampling time for control implementation was 5 minutes and the prediction horizon was set to 40 minutes. For the upper level MPC (UMPC), the control implementation time interval and averaging window were set to 30 minutes with a 12-hour prediction horizon. The temperature upper limit (T_u^U) followed the same night setup schedule. That is, 23.3^oC (74^oF) during the occupied period and 24.4^oC (76^oF during the unoccupied period. The lower temperature limits for both LMPC and UMPC (T_l^U and T_l^L) were set to 21.1^oC (70^oF). The NOAA API was used to retrieve weather forecasts (using the Purdue airport weather station, which is around 1.5 miles away from the lab) for the UMPC's 12-hr ahead prediction and the forecast was updated every 30 min, which is the UMPC implementation time. Once a decision was made by the UMPC, it was applied to the LMPC according to Eqn. (4). Then, a stage decision was made by the LMPC, and was transmitted to the thermostats every 5 minutes, which is the control implementation time interval for the LMPC.

Performance indexes: The HVAC energy cost savings, peak demand savings for both anytime demand

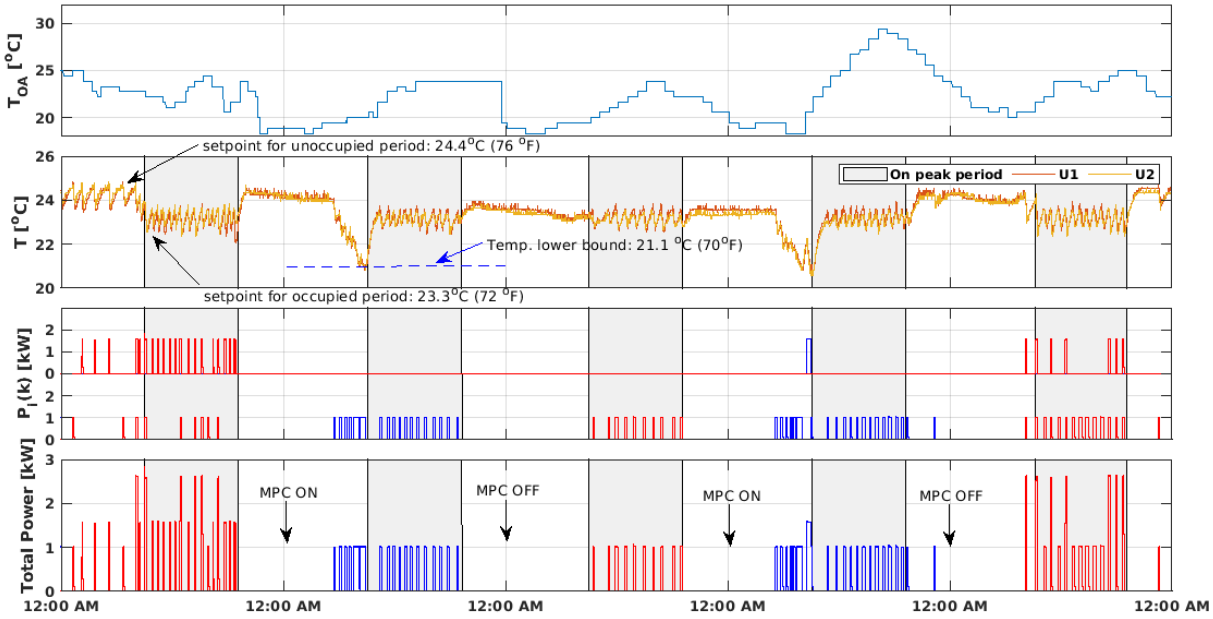

Figure 7: Sample profiles of outdoor air temperature, zone air temperature, setpoints, instantaneous unit powers, and total HVAC power under conventional control and MPC (Test I)

and on-peak demand cases, and thermostat temperatures were considered as performance metrics. To calculate HVAC energy cost for each controller, the utility price signal was multiplied with total HVAC power consumption. Because the demand charge is typically based on a 15-min averaged power rather than an instantaneous power, we first moving averaged the instantaneous, total HVAC power with a 15-min window, and then the maximum value was selected. Temperatures were directly measured from the thermostats.

5.1.3. Utility Cost Setup

The utility cost is a key parameter that decides the behavior and energy cost savings of the MPC. During this project, two electricity rates were investigated.

- Test I : 0.30 $/kWh from 9:00 AM to 9:00 PM (the ON peak period), and 0.10 $/kWh at other times.
- Test II: 0.20 $/kWh from 1:00 PM to 6:00 PM (the ON peak period), and 0.10 $/kWh at other times.

5.2. Experimental Test I (ON-to-OFF peak price ratio of 3)

5.2.1. Experimental Results: Short-Term Comparison

Fig. 7 shows sample test results for 5 days for the conventional control and MPC on mild days in June. As shown at the bottom of the figure, the two control algorithms were switched back and forth on a daily basis. The outdoor air temperature is shown in the first subfigure. Thermostat temperatures (red line: U1, yellow line: U2) are shown in the second subfigure. The grey-shaded area shows the on-peak price period. The instantaneous unit powers are displayed in the third figure and the total HVAC power (the sum of the

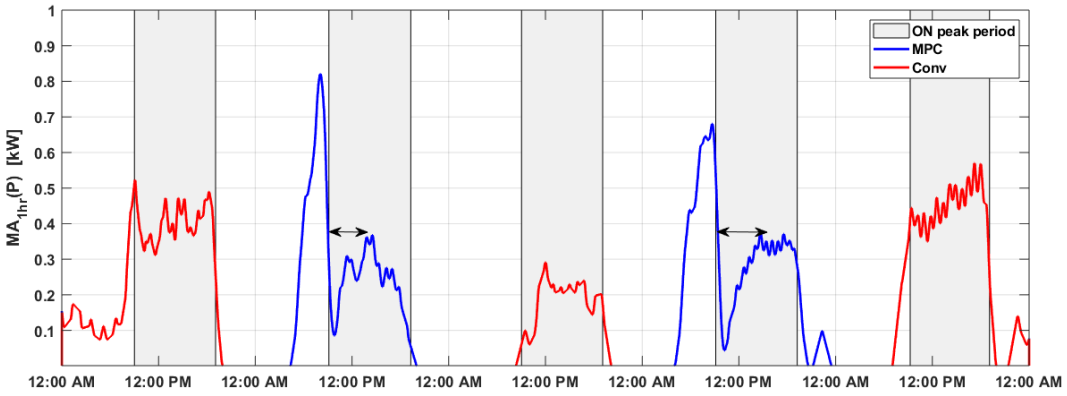

Figure 8: Profiles of a 1-hr moving averaged total HVAC power between the conventional control and MPC (Test I)

two powers) is shown in the last (red: conventional controller days, blue: the proposed controller, i.e. MPC, days).

The temperatures in the second figure show that the MPC clearly responds to the on-off peak price signal (0.3 \$/kWh from 9:00 AM- 9:00 PM, 0.1 \$/kWh elsewhere). The MPC precools the space until the temperatures hit the lower temperature limit (21.1^oC, 70^oF) when the electricity price is low, and turns off the units for a period after the price jumps. The precooling started at around 3 to 5 hours ahead of the price jump and the temperatures were smoothly lowered down. Note that even though the MPC precools the space, the peak HVAC power for the MPC days does not exceed that of the conventional control days. This result demonstrates that the hierarchical MPC is able to shift load by the UMPC while preventing unnecessary peaks by the LMPC. Recall that a typical MPC strategy which lowers setpoints for precooling but without coordinating unit operations is likely to activate all staged units during a precooling period due to a narrow thermostat deadband (0.56^oC, 1^oF) resulting in significant peak demand and discouraging building owners from participating in utility-based demand response programs.

It is particularly interesting and important for utility companies to see whether the MPC can actually shift electrical loads. In order to see how an electrical load behaves, a 1-hr moving average filter was applied to the instantaneous power signal and the outcome is plotted in Fig. 8. Electrical load profiles for the MPC clearly show a different pattern than those for the Conv. The MPC shifts electrical load for about 4 hours (the time periods indicated by double arrows in the figure).

5.2.2. Experimental Results: Long Term Comparison

To provide further reliability and performance assessment of the proposed load shifting algorithm, Test I experiments continued for an entire month of July. Fig. 9 shows sets of daily HVAC power profiles (1-hr moving averaged) for the conventional control (top) and MPC (bottom). $MA_{1hr}(P)$ means the 1-hr moving average on the total power measurements. To generate those plots, the daily load profiles were obtained from the month-long data and were classified into two groups corresponding to the Conv and MPC days. Different colors represent daily load profiles for different days, and the thick black line indicates the mean profile behavior over the 15 daily profiles for each controller as a representative profile.

Fig. 10 shows the comparison of the two representative profiles between the two controllers. These results from the analysis approach clearly show the charging and discharging processes of the building thermal mass

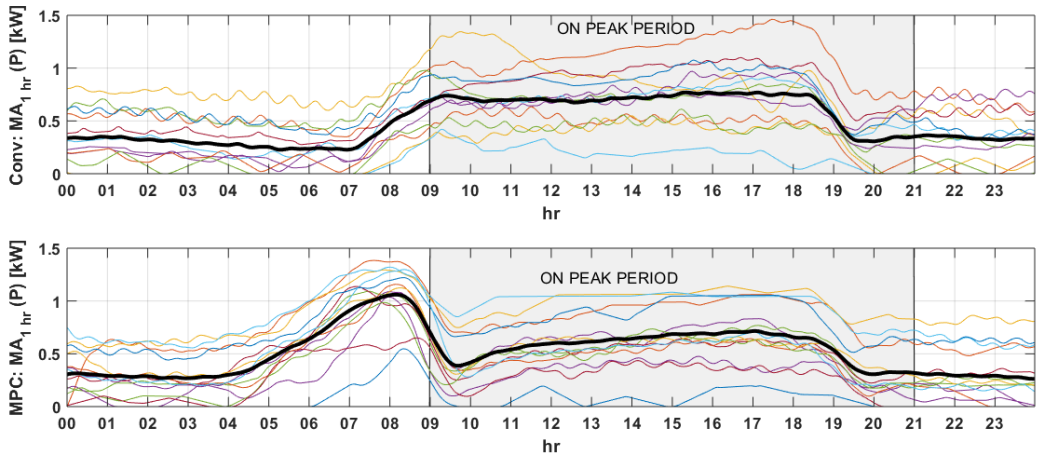

Figure 9: Distributions of daily profiles of total 1-hr moving average HVAC power for the conventional control and MPC (Test I). For each figure, different colors represent moving-averaged power measurements for different days, and the thick black line indicates the mean trajectory.

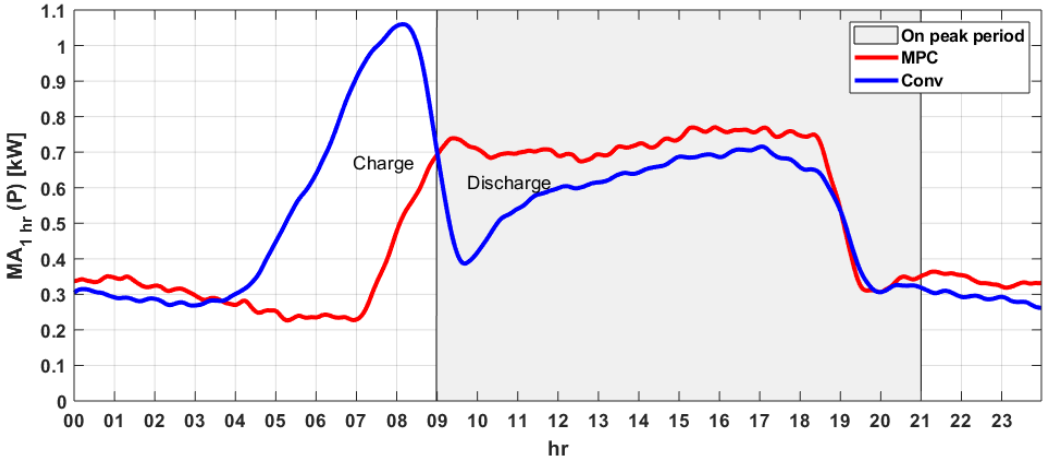

Figure 10: Comparison of daily profiles of total 1-hr moving average HVAC power between the conventional control and MPC (Test I)

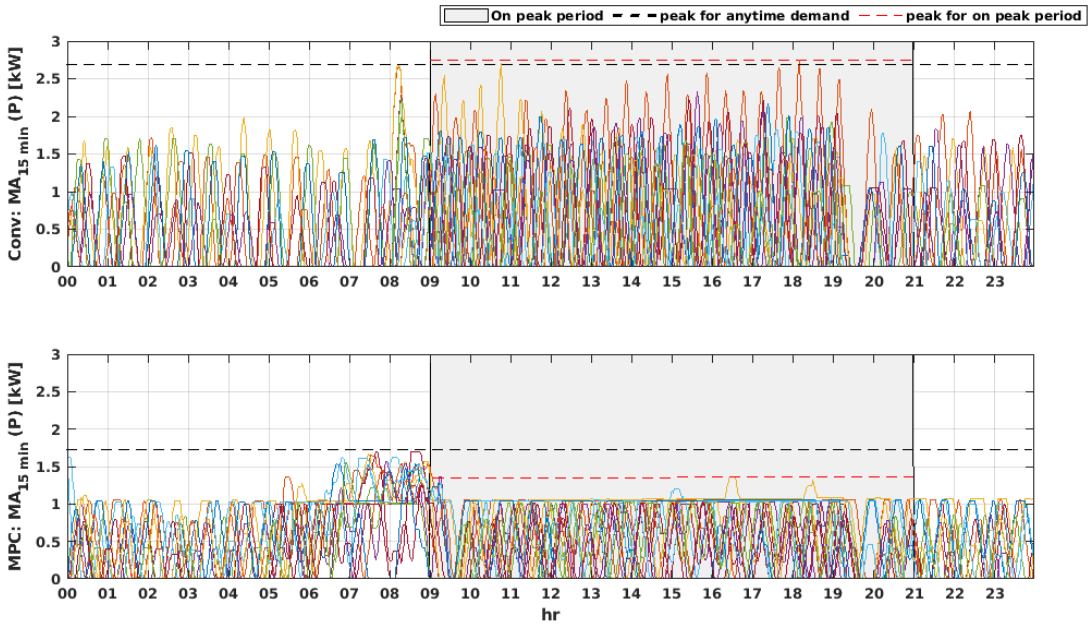

Figure 11: Distributions of daily profiles of total 15-min moving-average HVAC power for the conventional control and MPC (Test I). For each figure, different colors represent moving-averaged power measurements for different days.

which are not directly measurable. The MPC gradually increases the charging rate until the price jumps and it discharges after that. The discharging capacity (the difference between the two plots) is high at the beginning but drops exponentially, which is caused by the building's structural temperature that converges to the zone air temperature exponentially. The discharging process is effective for around 4 hrs (9:00 AM – 1:00 PM). Note that the charging energy (the area between the blue and red lines during the charging process) is much higher than the discharging energy. This makes sense since the lower zone air temperature for precooling brings more cooling load from the outdoor air. The MPC consumed more energy than the Conv by 7.38%.

The energy cost savings for the month experiment was 8.67%. The savings are somewhat lower than what was expected. It may be due to 1) a carpet and mat on the concrete floor for the conference room, 2) load prediction errors, 3) the long on-peak period, and 4) the ON to OFF peak cost ratio: That is, the price ratio of 3 may not be sufficient enough to overcome the increased building loads during the precooling process for the building.

Fig. 11 shows 15-minute moving averaged total power profiles for the two controllers to compare peak demand charges, since demand charges are often applied to a 15-minute average power. Depending on the utility, demand charges can be applied to just an on-peak period or both on-peak and off-peak periods. The black dashed lines Fig. 11 are the maximum values of the 15-minute moving averages over the all hours. The MPC's savings for anytime demand and on-peak demand are 38% and 46%, respectively. The Conv shows significantly higher anytime peak demand even though the Conv does not precool the space. This is because of the lack of coordination between units and the high correlation between operation of the two units caused by the significant inter-zonal coupling through the open area (See Fig. 5). As shown in the second subfigure,

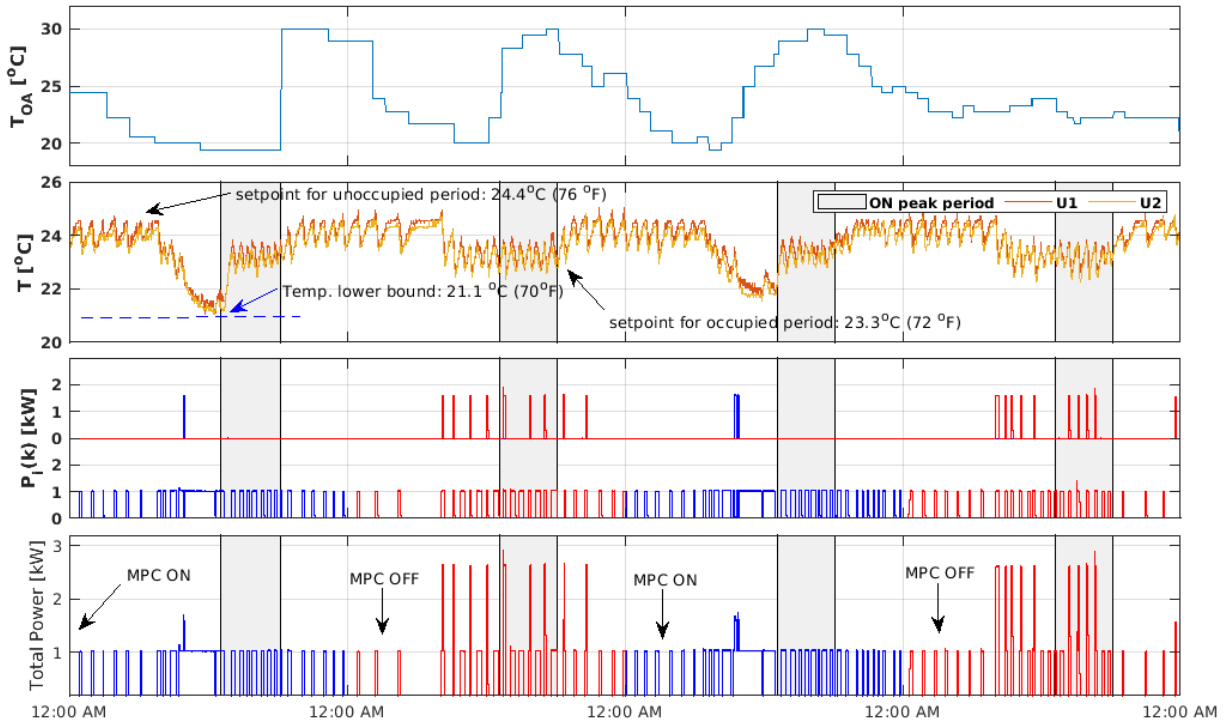

Figure 12: Sample profiles of outdoor air temperature, zone air temperature, setpoints, instantaneous unit powers, and total HVAC power under conventional control and MPC (Test II)

the MPC supervises the operation of units to reduce peaks even for precooling.

5.3. Experimental Test II (ON-to-OFF peak price ratio of 2)

5.3.1. Experimental Results: Short-Term Comparison

Fig. 12 shows sample test results for 4 days for the conventional control and MPC on days in August under the ON-to-OFF peak price ratio of 2 and an on-peak period from 1:00 PM to 6:00 PM. As shown at the bottom of the figure, the two control algorithms were switched back and forth on a daily basis. Thermostat temperatures (blue line: U1, brown line: U2) are shown in the second subfigure. The unit powers are displayed in the third figure and the total HVAC power (a 15-min moving average) is shown in the last (red: conventional controller days, blue: the MPC days).

Like Test I, the temperatures in the second figure show that the MPC clearly responds to the on-off peak price signal (0.2 \$/kWh from 1:00 PM- 6:00 PM, 0.1 \$/kWh elsewhere). The MPC precools the space down to the lower temperature limit (21.1^oC, 70^oF) when the electricity price is low, and turns off the units for a period after the price jumps. The precooling started at around 2 to 4 hours ahead of the price jump and the temperatures were smoothly lowered down. During the precooling periods, the peaks are under regulation as shown in the bottom of the figure.

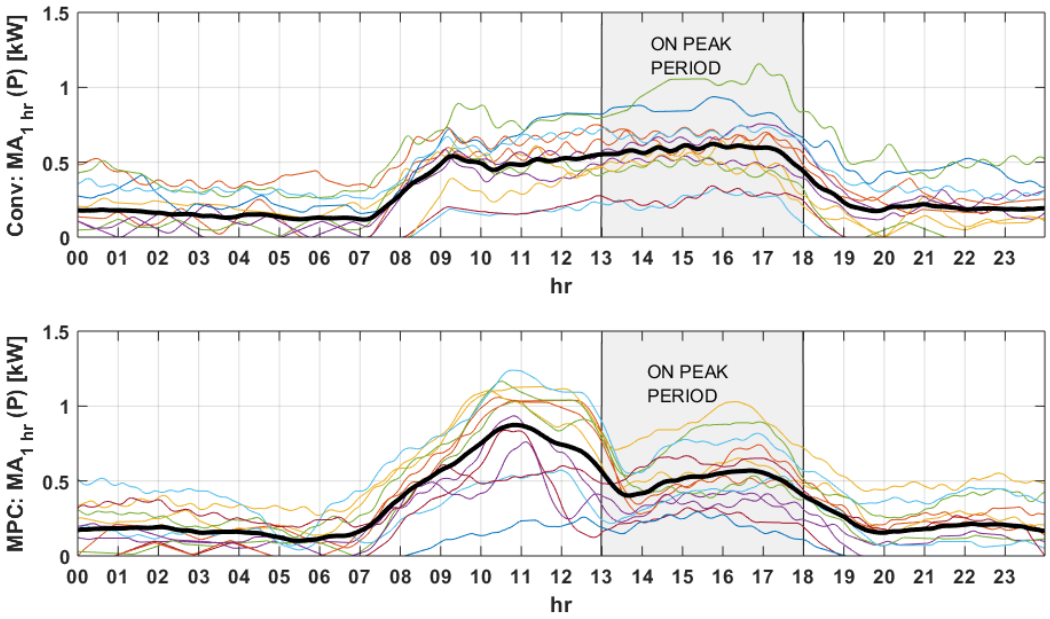

Figure 13: Distributions of daily profiles of total 1-hr moving average HVAC power for the conventional control and MPC (Test II). For each figure, different colors represent moving-averaged power measurements for different days, and the thick black line indicates the mean trajectory.

5.3.2. Experimental Results: Long Term Comparison

Fig. 13 shows sets of daily HVAC power profiles (1-hr moving averaged) for the conventional and MPC. Fig. 14 shows comparisons of the two representative profiles between the two controllers. To ensure that the comparison of sampled powers is meaningful, daily temperature distributions are also provided in Fig. 15. Clearly, the MPC regulated thermostat temperatures within the specified temperature range (21.1 to 23.3^oC, 70 to 74^oF during the occupied period of 9:00 AM to 6:00 PM, and 21.1 to 24.4^oC, 70 to 76^oF during the unoccupied period). As shown in the last subfigure of Fig. 15, the MPC precooled the space to around 22.2^oC (72^oF) although the lower limit was set to 21.1^oC (70 ^oF). This is due to the two conflicting driving potentials of the MPC, i.e., the utility cost rate structure and increment of loads from the outdoor air for precooling.

Fig. 14 demonstrates the electrical load shifting capability of the MPC. It shifts electrical loads for about 3 to 4 hours. The MPC gradually increases the charging until the price jump and it discharges after that. The discharging capacity is high at the beginning but drops exponentially. The discharging process is effective for around 4 hrs (1:00 PM – 5:00 PM). The increase of energy consumption associated with the precooling compared with that of the baseline is 9.77%. For the Test I case, it was 7.38%. The increment could be explained by higher outdoor air temperature during the precooling time (the precooling occurs early morning and late morning for TEST I and II, respectively).

The energy cost savings for this experiment was only 3.61%. The savings was significantly reduced from that for the Test I case (8.67%) which is mainly due to the reduced ON-to-OFF peak price ratio of 2 from 3. As mentioned, the small energy cost savings are due to a significant thermal resistance between the

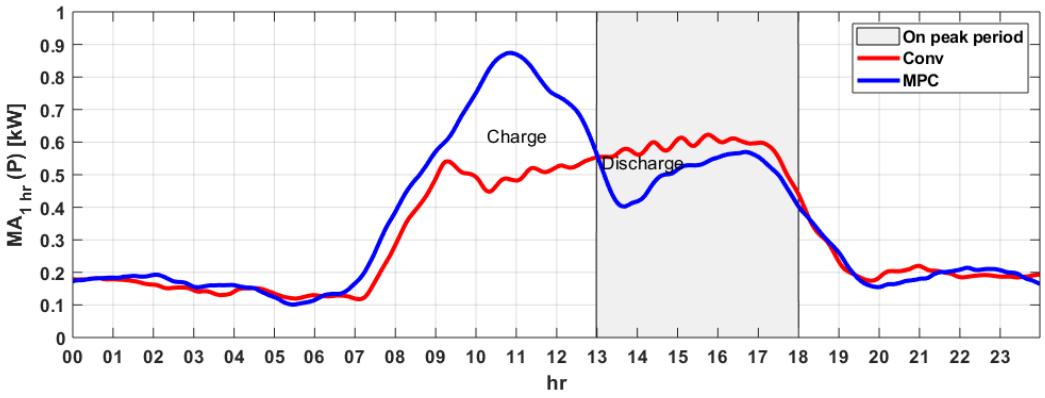

Figure 14: Comparison of representative daily profiles of total 1-hr moving average HVAC power between the conventional control and MPC (Test II)

zone air and building structure and poor insulation. Fig. 16 shows 15-min moving averaged total power profiles for the two controllers to compare peak demand charges. The MPC's anytime demand savings are 36% (compare the black dashed lines showing the maximum values for the two controllers). For the case of on-peak demand charge, savings are 60% (see the red dashed lines showing the maximum peaks over the on-peak period). The greater on-peak demand savings are the combined effect of reduced cooling loads due to precooling and the narrower on-peak period where the discharging is effective in addition to the LMPC's coordination effort.

5.4. Further Discussion and Lessons Learned

The charging and discharging figures (Fig. 10 and 14) provide important demonstrations of the use of buildings' inherent energy storage, i.e., the thermal mass.

First, the shifted load during an ON-peak price period is effective for around 4 hours but the profile is limited to an exponentially decreasing curve. As mentioned, this is because of the natural thermodynamic and heat transfer processes where the temperature of the thermal mass converges to the zone air temperature which is bounded by a comfort limit.

Second, the *round-trip efficiency* of the thermal mass is not 100% and depends on not only the thermal capacitance of the mass but also the thermal resistances between the zone air and mass and between the zone air and outdoor temperature, and the precooling time. Recall that the charging energy is much higher than the discharging energy: the charging energy was around 1.5 times higher than the discharging energy for the Test I (the ON-to-OFF peak price ratio of 3 where the ON peak starts from 9:00 AM), and more than 2 times higher for the Test II (the ON-to-OFF peak price ratio of 2 where the ON peak starts from 1:00 PM). This leads to round-trip efficiencies of less than 70% and 50%, respectively. The poor round-trip efficiency is because the lower zone air temperature during precooling brings more cooling load from the outdoor air. In addition, as mentioned in Section 5.1 and shown in Fig. 4, the test space has a carpet and mat and has large single-pane windows. From the heat transfer point of view, it is clear that the relatively higher thermal resistance between the zone air and structural mass and the lower resistance between the zone air and outdoor make it easier for the *cooling energy* supplied for precooling to be offset by increasing heat gains from the outdoor air. To further support this, we refer to Ruud et al. (1990) who tested a precooling strategy for an existing building. They reported a substantial increase in the total cooling required and no

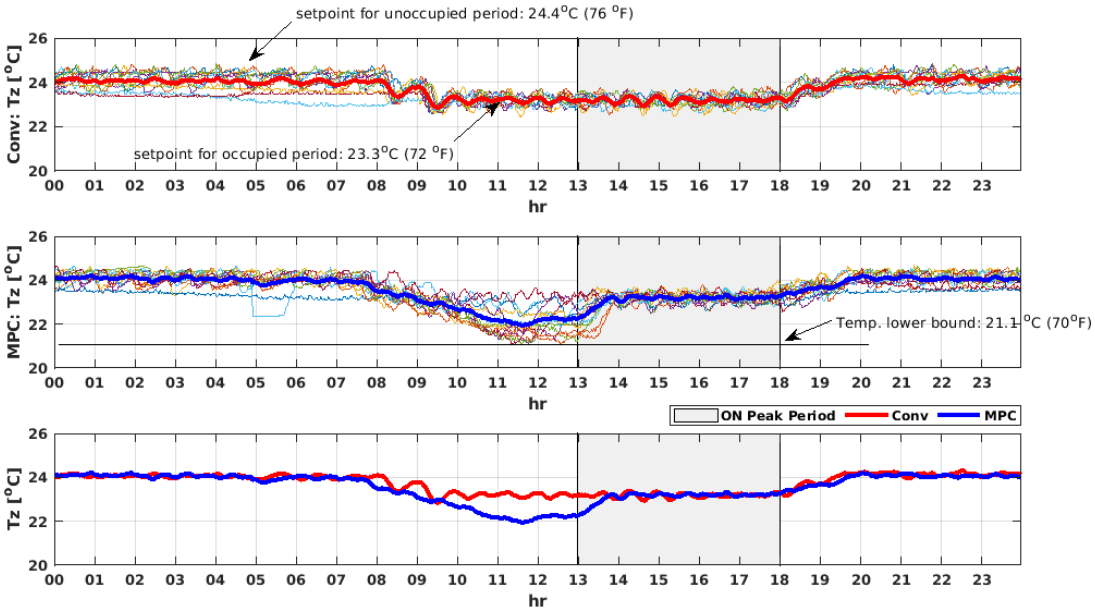

Figure 15: Distributions of daily temperature profiles between the conventional control and MPC (Test II). For each figure, different colors represent thermostat temperature measurements for different days, and the thick black line indicates the mean trajectory.

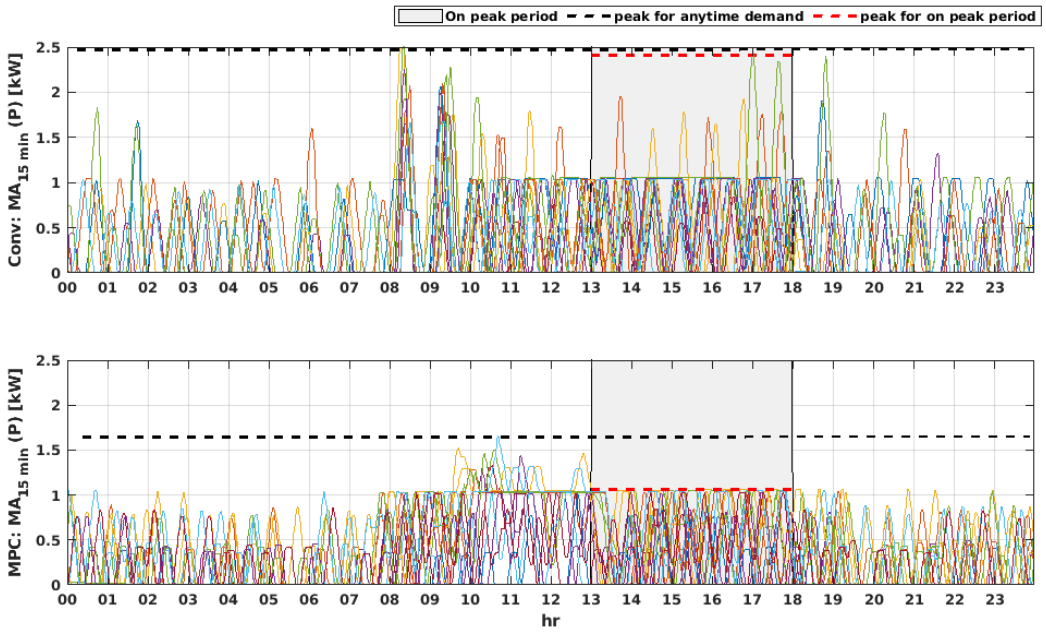

Figure 16: Distributions of daily profiles of total 15-min moving average HVAC power for the conventional control and MPC (Test II). For each figure, different colors represent moving-averaged power measurements for different days.

reduction in the peak cooling requirement, due to a relatively light building structure, weak heat transfer coupling between the thermal mass and room air, and strong heat transfer coupling to external ambient conditions.

Third, the results (Fig. 10 and 14) indicate that the trade-off for load flexibility using the thermal mass is energy efficiency. Again, this is because, for cooling load shifting using the thermal mass, room setpoints have to be lowered bringing more cooling load from the outdoor compared with the conventional, fixed setpoint case. Of course, the higher unit COP for the precooling period could compensate for the increased thermal load, but the effect was not significant in our test cases.

The MPC would show higher and reliable utility cost savings and lower energy penalties for well-insulated buildings (e.g., newly built or retrofitted buildings) compared with poorly-insulated buildings. For the latter, it is difficult to achieve sufficient energy cost savings and special care for modeling is needed for MPC implementation, otherwise the poor round trip efficiency could result in negative energy cost savings. In this case, the only reliable utility cost savings potential for SMCBs comes from the demand savings through coordinating unit stages as demonstrated in Section 5.2.2 and 5.3.2.

6. Conclusions

Despite a long history of studying MPCs applied to buildings and increasing needs for load flexibility in small and medium sized commercial buildings (SMCB), few advanced control algorithms have been developed for SMCBs. This paper discussed the unique MPC challenge of high peak demand occurring when shifting HVAC load for SMCBs served by multiple staged packaged air conditioners, and presented a hierarchical

MPC to overcome this issue. The load shifting capability of the MPC while regulating the unnecessary peaks during precooling has been tested for a laboratory space over two months for two different time-of-use (TOU) scenarios. The MPC successfully shifted electrical loads in response to TOU rates, with remarkable HVAC demand cost savings, anytime demand cost savings over 30% and on-peak demand cost savings over 40%, but with only modest energy cost savings. The virtual battery, i.e. the building thermal mass, was effective for about 4-5 hours with a substantial load reduction during the ON peak period. The energy cost savings were less than 10%. One of the reasons for the low energy cost savings is the fact that the site has a carpet, mat and a poor envelope with single pane windows which results in inefficient charging and discharging of the building mass. It is expected that savings should be significantly greater for more typical commercial buildings.

7. ACKNOWLEDGMENTS

The work was supported by the Center for High Performance Building (CHPB) at Purdue University, and completed with the support of the Assistant Secretary for Energy Efficiency and Renewable Energy, Building Technologies Office of the U.S. Department of Energy under Contract No. DE-AC02-05CH11231.

References

Andersen, K.K., Madsen, H., Hansen, L.H., 2000. Modelling the heat dynamics of a building using stochastic differential equations. Energy and Buildings 31, 13–24.

Avci, M., Erkoc, M., Rahmani, A., Asfour, S., 2013. Model predictive hvac load control in buildings using real-time electricity pricing. Energy and Buildings 60, 199–209.

Bianchini, G., Casini, M., Pepe, D., Vicino, A., Zanvettor, G.G., 2017. An integrated mpc approach for demand-response heating and energy storage operation in smart buildings, in: 2017 IEEE 56th Annual Conference on Decision and Control (CDC), IEEE. pp. 3865–3870.

Bianchini, G., Casini, M., Vicino, A., Zarrilli, D., 2016. Demand-response in building heating systems: A model predictive control approach. Applied Energy 168, 159–170.

Biyik, E., Brooks, J.D., Sehgal, H., Shah, J., Gency, S., 2015. Cloud-based model predictive building thermostatic controls of commercial buildings: Algorithm and implementation, in: American Control Conference (ACC), 2015, IEEE. pp. 1683–1688.

Braun, J., 1990. Reducing energy costs and peak electrical demand through optimal control of building thermal mass. ASHRAE Transactions 92, 876–888.

Braun, J., Chaturvedi, N., . An inverse gray-box model for transient building load prediction. HVAC&R Research 8, 73–99. URL: http://www.tandfonline.com/doi/abs/10.1080/10789669.2002.10391290, doi:10.1080/10789669.2002.10391290.

Braun, J.E., Montgomery, K.W., Chaturvedi, N., 2001. Evaluating the performance of building thermal mass control strategies. HVAC&R Research 7, 403–428.

Cai, J., Braun, J.E., 2018. Assessments of variable-speed equipment for packaged rooftop units (rtus) in the united states. Energy and Buildings 164, 203–218.

Candanedo, J., Dehkordi, V., Stylianou, M., 2013. Model-based predictive control of an ice storage device in a building cooling system. Applied Energy 111, 1032–1045.

Ceusters, G., Rodríguez, R.C., García, A.B., Franke, R., Deconinck, G., Helsen, L., Nowé, A., Messagie, M., Camargo, L.R., 2021. Model-predictive control and reinforcement learning in multi-energy system case studies. Applied Energy 303.

Chen, X., Wang, Q., Srebric, J., 2015. Model predictive control for indoor thermal comfort and energy optimization using occupant feedback. Energy and Buildings 102, 357–369.

Dong, B., Lam, K.P., Neuman, C., 2011. Integrated building control based on occupant behavior pattern detection and local weather forecasting, in: Twelfth International IBPSA Conference. Sydney: IBPSA Australia, pp. 14–17.

Drgoňa, J., Arroyo, J., Figueroa, I.C., Blum, D., Arendt, K., Kim, D., Ollé, E.P., Oravec, J., Wetter, M., Vrabie, D.L., et al., 2020. All you need to know about model predictive control for buildings. Annual Reviews in Control .

Fraisse, G., Viardot, C., Lafabrie, O., Achard, G., 2002. Development of a simplified and accurate building model based on electrical analogy. Energy and buildings 34, 1017–1031.

Harb, H., Boyanov, N., Hernandez, L., Streblow, R., Müller, D., 2016. Development and validation of grey-box models for forecasting the thermal response of occupied buildings. Energy and Buildings 117, 199–207.

Hilliard, T., Kavgic, M., Swan, L., 2016. Model predictive control for commercial buildings: trends and opportunities. Advances in Building Energy Research 10, 172–190.

Katipamula, S., Underhill, R.M., Goddard, J.K., Taasevigen, D., Piette, M., Granderson, J., Brown, R.E., Lanzisera, S.M., Kuruganti, T., 2012. Small-and medium-sized commercial building monitoring and controls needs: A scoping study. Pacific Northwest National Laboratory (PNNL), Richland, WA (US), Tech. Rep .

Killian, M., Kozek, M., 2016. Ten questions concerning model predictive control for energy efficient buildings. Building and Environment 105, 403–412.

Kim, D., Braun, J., Cai, J., Fugate, D., 2015. Development and experimental demonstration of a plug-and-play multiple rtu coordination control algorithm for small/medium commercial buildings. Energy and Buildings 107, 279–293.

Kim, D., Braun, J.E., 2018. Development, implementation and performance of a model predictive controller for packaged air conditioners in small and medium-sized commercial building applications. Energy and Buildings 178, 49–60.

Kim, D., Cai, J., Ariyur, K.B., Braun, J.E., 2016. System identification for building thermal systems under the presence of unmeasured disturbances in closed loop operation: Lumped disturbance modeling approach. Building and Environment 107, 169–180.

Kim, D., Cai, J., Braun, J.E., Ariyur, K.B., 2018. System identification for building thermal systems under the presence of unmeasured disturbances in closed loop operation: Theoretical analysis and application. Energy and Buildings 167, 359 – 369. URL: http://www.sciencedirect.com/science/article/pii/S0378778817317322, doi:https://doi.org/10.1016/j.enbuild.2017.12.007.

Kim, D., Wang, Z., Brugger, J., Blum, D., Wetter, M., Hong, T., Piette, M.A., 2022. Experimental demonstration and site performance evaluation of mpc for a large chiller plant with tes for renewable energy integration and grid decarbonization. Applied Energy (Submitted) .

Li, S., Joe, J., Hu, J., Karava, P., . System identification and model-predictive control of office buildings with integrated photovoltaic-thermal collectors, radiant floor heating and active thermal storage. Solar Energy 113, 139–157. URL: https://linkinghub.elsevier.com/retrieve/pii/S0038092X14005684, doi:10.1016/j.solener.2014.11.024.

Nutaro, J.J., Fugate, D.L., Kuruganti, T., Starke, M.R., 2014. An inexpensive retrofit technology for reducing peak power demand in small and medium commercial buildings, Conference: 3rd International High Performance Buildings Conference at Purdue.

Oldewurtel, F., Ulbig, A., Morari, M., Andersson, G., 2011. Building control and storage management with dynamic tariffs for shaping demand response, in: 2011 2nd IEEE PES International Conference and Exhibition on Innovative Smart Grid Technologies, IEEE. pp. 1–8.

Oldewurtel, F., Ulbig, A., Parisio, A., Andersson, G., Morari, M., 2010. Reducing peak electricity demand in building climate control using real-time pricing and model predictive control, in: 49th IEEE conference on decision and control (CDC), IEEE. pp. 1927–1932.

Patteeuw, D., Henze, G.P., Helsen, L., 2016. Comparison of load shifting incentives for low-energy buildings with heat pumps to attain grid flexibility benefits. Applied energy 167, 80–92.

Putta, V., Kim, D., Cai, J., Hu, J., Braun, J.E., 2015. A switched dynamic programming approach towards optimal control of multiple rooftop units, in: American Control Conference (ACC), 2015, IEEE. pp. 281–287.

Qureshi, F.A., Jones, C.N., 2018. Hierarchical control of building hvac system for ancillary services provision. Energy and Buildings 169, 216–227.

Reynders, G., Diriken, J., Saelens, D., 2014. Quality of grey-box models and identified parameters as function of the accuracy of input and observation signals. Energy and Buildings 82, 263–274.

Risbeck, M.J., Maravelias, C.T., Rawlings, J.B., Turney, R.D., 2017. A mixed-integer linear programming model for real-time cost optimization of building heating, ventilation, and air conditioning equipment. Energy and Buildings 142, 220–235.

Rockett, P., Hathway, E.A., 2017. Model-predictive control for non-domestic buildings: a critical review and prospects. Building Research & Information 45, 556–571.

Rogers, D., Foster, M., Bingham, C., 2014. Experimental investigation of a recursive modelling mpc system for space heating within an occupied domestic dwelling. Building and Environment 72, 356–367.

Ruud, M., Mitchell, J., Klein, S., 1990. Use of building thermal mass to offset cooling loads. ASHRAE Transactions (American Society of Heating, Refrigerating and Air-Conditioning Engineers);(United States) 96.

Seem, J., House, J., 2010. Development and evaluation of optimization-based air economizer strategies. Applied Energy 87, 910–924.

Širokỳ, J., Oldewurtel, F., Cigler, J., Prívara, S., 2011. Experimental analysis of model predictive control for an energy efficient building heating system. Applied Energy 88, 3079–3087.

Skogestad, S., Postlethwaite, I., 2007. Multivariable feedback control: analysis and design. volume 2. Citeseer.

Taylor, S.T., Cheng, C., 2010. Why enthalpy economizers don't work. ASHRAE Journal 52, 12–28.

Vrettos, E., Lai, K., Oldewurtel, F., Andersson, G., 2013. Predictive control of buildings for demand response with dynamic day-ahead and real-time prices, in: 2013 European Control Conference (ECC), IEEE. pp. 2527–2534.

Wang, W., Katipamula, S., Ngo, H., Underhill, R., 2019. Energy performance evaluation of variable-speed packaged rooftop units using field measurements and building energy simulation. Energy and Buildings 183, 118–128.

Wang, W., Katipamula, S., Ngo, H., Underhill, R., Taasevigen, D., Lutes, R., 2013. Advanced rooftop control (arc) retrofit: Field-test results. PNNL-22656, Pacific Northwest National Laboratory .

Zhang, X., Pipattanasomporn, M., Rahman, S., 2017. A self-learning algorithm for coordinated control of rooftop units in small-and medium-sized commercial buildings. Applied Energy 205, 1034–1049.